IOPscience iopscience.iop.org

Home Search Collections Journals About Contact us My IOPscience

Polar and magnetoelectric multipoles in gallium ferrate inferred from optical and x-ray measurements

This article has been downloaded from IOPscience. Please scroll down to see the full text article.

2007 J. Phys.: Condens. Matter 19 376205

(http://iopscience.iop.org/0953-8984/19/37/376205)

View the table of contents for this issue, or go to the journal homepage for more

Download details:
IP Address: 129.252.86.83
The article was downloaded on 29/05/2010 at 04:41

Please note that terms and conditions apply.

IOP PUBLISHING JOURNAL OF PHYSICS: CONDENSED MATTER

J. Phys.: Condens. Matter **19** (2007) 376205 (13pp) doi:10.1088/0953-8984/19/37/376205

# Polar and magnetoelectric multipoles in gallium ferrate inferred from optical and x-ray measurements

**Stephen W Lovesey**[1,2], **Kevin S Knight**[1,3] **and Ewald Balcar**[4]

[1] ISIS Facility, RAL, Oxfordshire OX11 0QX, UK
[2] RIKEN Harima Institute, SPring-8, Hyogo 679-5148, Japan
[3] Department of Mineralogy, The Natural History Museum, London SW7 5BD, UK
[4] Vienna University of Technology, Atominstitut, Stadionallee 2, A-1020 Vienna, Austria

Received 13 July 2007
Published 22 August 2007
Online at stacks.iop.org/JPhysCM/19/376205

**Abstract**

Observations utilizing optical and x-ray techniques of coexisting magnetoelectric, piezoelectric and magnetic modifications in gallium ferrate ($GaFeO_3$) are successfully analysed with an atomic model that complies with the established chemical structure and the motifs of spontaneous polar and ferrimagnetic order. Electron variables in the corresponding scattering length, which is common to an analysis of dichroism and diffraction, are expressed as multipoles for charge, magnetic, magnetoelectric and polar electron degrees of freedom. Polar and magnetoelectric multipoles are parity-odd and cannot exist in a compound with a centrosymmetric structure. Magnetoelectric multipoles are time-odd and vanish with loss of long-range magnetic order. Dichroic signals measured in the energy region 1.0–2.5 eV and near the Fe K edge are consistent with a sum of magnetochiral and non-reciprocal linear signals caused by magnetoelectric multipoles in E1–M1 and E1–E2 absorption events. Resonant x-ray Bragg diffraction near the Fe K edge shows interference not previously reported between Thomson scattering and resonant E1, M1 and E2 processes.

## 1. Introduction

Spontaneous polar and magnetic order coexist in gallium ferrate ($GaFeO_3$). The multiferroic properties of the compound have been extensively studied since 1960, when it was first prepared and characterized [1], by many different experimental techniques. Collinear ferrimagnetism [2] develops below a critical temperature $T_c \approx 200$ K, which depends on the relative concentrations of gallium and iron. Rado [3] observed a large linear magnetoelectric effect, and the induced polarization is normal to the applied magnetic field.

The non-centrosymmetric structure of $GaFeO_3$ has an orthorhombic unit cell with $a \approx 8.8$, $b \approx 9.4$ and $c \approx 5.1$ Å, that belongs to the $C_{2v}$ polar crystal class, and a magnetic point group $m'2'm$ [4]. The space group is $Pc2_1n$ which indicates a spontaneous polarization along the $b$-axis. Below $T_c$, antiferromagnetically coupled Fe magnetic moments align along the

 © 2007 IOP Publishing Ltd Printed in the UK 

$c$-axis, with $Pc'2'_1n$ the magnetic space group [2]. The compound is a ferrimagnet because Fe occupations at Fe-rich sites are slightly different.

Quite recently, untwinned large single crystals of $GaFeO_3$ have been prepared [5] and studied by both optical and x-ray techniques [6–8]. Studies made with instruments at the Photon Factory (KEK, Japan), with linearly polarized x-rays, include measurements near the Fe K edge of dichroic signals [6] and resonant Bragg diffraction [8]. In all the experiments, the sample was subjected to an alternating magnetic field, parallel to the magnetic easy axis, and data sets collected in fields of opposite polarity were subtracted. Such difference data are proportional to time-odd multipoles that vanish in the absence of long-range magnetic order. The crystal was initially held at a temperature of 50 K. Difference data were found to continuously diminish in intensity with increasing temperature of the sample and to vanish above $T_c$.

We find that, the dichroic signals measured in the x-ray region and the optical region (an energy region of 1.0–2.5 eV) can be attributed to a sum of two non-reciprocal signals that are often called magnetochiral dichroism (M$\chi$D) and non-reciprocal linear dichroism (NRLD) [9–12]. Observed signals are therefore a direct measure of the Fe anapole, and other magnetoelectric multipoles that are both parity-odd and time-odd. The observed resonant x-ray Bragg diffraction [8] is possibly even more intriguing because it appears to reveal interference between parity-odd events in the Fe pre-edge region, where E2 events hold sway, and the region of main absorption delivered by E1 events.

Our work on gallium ferrate uses the established structural [4] and magnetic symmetry [2, 5] to construct an atomic model of the compound. We then calculate structure factors for parity-even events (E1–E1 and E2–E2) and parity-odd events (E1–M1 [9, 11, 13] and E1–E2). The corresponding scattering length provides estimates of integrated dichroic signals and, also, Bragg diffraction intensities [13, 14] that can be directly compared to observations on $GaFeO_3$.

## 2. Model structure factors

Time-odd or magnetic properties of $GaFeO_3$ are attributed to ferric ($3d^5$) $Fe^{3+}$ ions. The Fe moment is pure spin, to a very good approximation. The spin–orbit coupling can add a small amount of orbital moment to the $S = 5/2$ spin moment by mixing $^6$S and $^4$P terms, for example.

There are four cations in the asymmetric unit of the orthorhombic unit cell and the occupied sites (Wyckoff 4a in space group No. 33) have no point symmetry. In the unit cell illustrated in figure 1 there are two groups of almost octahedrally coordinated, inequivalent Fe sites with occupation probabilities $p_1 = 0.77$ and $p_2 = 0.70$. One of the two Ga groups, Ga2, is also octahedrally coordinated with Fe occupancy $p_3 = 0.35$, whereas Ga1 ($p_4 = 0.18$) has an almost tetrahedral oxygen coordination. In our future working we ignore the tetrahedrally coordinated Fe ion because of its relatively small contribution to physical quantities of interest.

Cation sites in an orthorhombic cell are at positions $(x, y, z)$, $(-x, 1/2 + y, -z)$, $(1/2 + x, 1/2 + y, 1/2 - z)$ and $(1/2 - x, y, 1/2 + z)$. Let $(x, y, z)$ be our reference site and consider the remaining sites, labelled 2, 3, and 4, in the order in which they are given. Environments at sites 1 and 2 are related through a rotation by $\pi$ about the $b$-axis, $C_{2b}$. Sites 3 and 4 are related to the environment of site 1 by mirror planes $m_c$ and $m_a$ normal to the $c$- and $a$-axis, respectively, and a mirror plane operation is the product of inversion and a rotation by $\pi$ about the axis normal to the plane. All Fe magnetic moments in a cell are observed to be parallel to the $c$-axis [5], and this configuration of moments is achieved, with reference to site 1, by the addition of the time-reversal operator at sites 2 and 4.

A multipole is the expectation value, or time average, of a spherical tensor operator and we denote the expectation value by angular brackets about the operator. The expectation value is

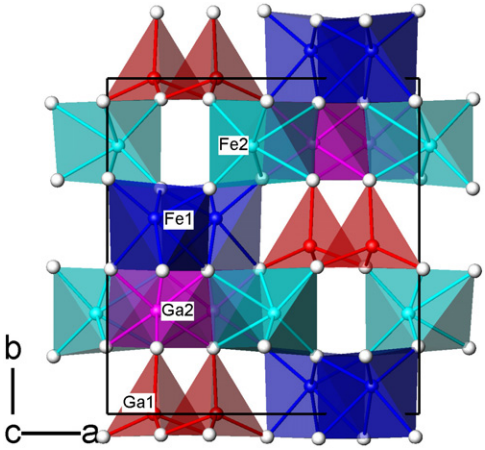


**Figure 1.** Crystal structure, in the $a$–$b$ plane, of $GaFeO_3$ showing the positions and environments of Ga1, Ga2, Fe1 and Fe2 ions. The $y$ parameter of Ga1 is set to zero. Displacements along the $b$ direction of Ga2 and Fe2 are opposite to the displacement along the $b$ direction of Fe1. Iron magnetic moments (not shown) are normal to the plane of the figure, and moment directions at sites Ga2 and Fe2 are opposite to the moment direction at Fe1.

(This figure is in colour only in the electronic version)

calculated with a valence state which accepts the photo-ejected electron in a specific absorption event, and thus a multipole is an equilibrium property of the ground state of the compound. Multipoles that describe parity-even events are not changed by the inversion operation. For this class of multipoles, there is a one to one correspondence between the multipole's rank, labelled by an integer $K$, and the behaviour of the multipole with respect to the reversal of time, namely, even (odd) rank multipoles are time-even (time-odd).

Our structure factor is created by the sum of four cation multipoles in an orthorhombic cell. If $\langle T^K_Q \rangle$ is the parity-even multipole for the Fe ion at site 1 in the cell,

$$\Psi^K_Q = \{1 + (-1)^{k+Q}\} \left\{ \langle T^K_Q \rangle + \langle T^K_{-Q} \rangle \right\}. \tag{2.1}$$

In the structure factor (2.1) we have included spatial phase factors that arise for Bragg diffraction at reflections $(0k0)$ where the Miller index $k$ is an integer. Note that $\Psi^K_Q$ is an even function of the projection $Q$ $(-K \leqslant Q \leqslant K)$ and it vanishes for even $k$ and odd $Q$. Complex conjugation satisfies $\langle T^K_Q \rangle^* = (-1)^Q \langle T^K_{-Q} \rangle$ and this property is common to all multipoles we use.

There are two classes of parity-odd multipoles. Multipoles $\langle U^K_Q \rangle$ are time-even and called polar, and $\langle G^K_Q \rangle$ are time-odd and called magnetoelectric. In particular, $\langle G^1_Q \rangle$ is the anapole moment whose components are related to the expectation value of the vector product of the orbital magnetic moment and the polarization, or electric field.

Parity-odd structure factors are

$$\Psi^{K,u}_Q = \{1 - (-1)^{k+Q}\} \left\{ \langle U^K_Q \rangle - (-1)^K \langle U^K_{-Q} \rangle \right\} \tag{2.2}$$

and

$$\Psi^{K,g}_Q = \{1 - (-1)^{k+Q}\} \left\{ \langle G^K_Q \rangle + (-1)^K \langle G^K_{-Q} \rangle \right\}. \tag{2.3}$$

Properties of note include: the difference between the structure factors (2.2) and (2.3) arises because of the configuration of magnetic moments, and $\Psi^{K,g}_Q$ vanishes in the absence

**Table 1.** Structure factors for Thomson scattering by gallium ferrate, $F_c = F_c' + \mathrm{i}F_c''$ include contributions from all cations and anions in the unit cell, and they are expressed in units of $r_e$. Dispersion terms for Fe do not appear here because they are included in the resonant contributions to scattering. Debye–Waller factors are not used in our calculations of $F_c$ for their effect is entirely negligible. Components in $A = A' + \mathrm{i}A''$ and $B = B' + \mathrm{i}B''$ are calculated from expression (2.8).

| | (020) | (040) | $(0\bar{4}0)$ |
|---|---|---|---|
| $F_c'$ | −6.78 | 81.50 | 87.65 |
| $F_c''$ | −45.31 | 109.93 | −103.55 |
| $A'$ | −0.45 | −0.09 | −0.09 |
| $A''$ | 0.03 | 1.68 | −1.68 |
| $B'$ | 1.23 | −0.66 | −0.66 |
| $B''$ | 1.30 | −0.34 | 0.34 |
| $A'F_c' + A''F_c''$ | 1.70 | 177.02 | 165.72 |
| $-A'B'' + A''B'$ | 0.61 | −1.13 | 1.13 |

of long-range magnetic order; parity-odd structure factors vanish for even $k + Q$; $\Psi^{K,u}_{-Q} = -(-1)^K \Psi^{K,u}_Q$ and $\Psi^{K,g}_{-Q} = (-1)^K \Psi^{K,g}_Q$.

Structure factors (2.1)–(2.3) are used for the Fe ions in group 1, Fe1. X-ray and neutron diffraction studies reveal that Fe magnetic moments at Fe2 sites and at Ga2 sites align along the $c$-axis in the opposite direction to the moments at Fe1 sites, and the signatures for magnetic moments also applies to polarizations found along the $b$-axis. In consequence, bulk electric and magnetic properties associated with the three groups of inequivalent cations, Fe1, Fe2 and Ga2, can be described in terms of the structure factors (2.1)–(2.3) and three structure factors derived from them by a rotation through $\pi$ about the $a$-axis, $C_{2a}$. The property $C_{2a}\Psi^K_Q = (-1)^K \Psi^K_{-Q}$ actually holds for any spherical tensor. Adding structure factors for the three inequivalent groups of cations, together with spatial phase factors appropriate for the reflection $(0k0)$, we arrive at our working model that is specified by four structure factors,

$$\Psi^K_Q \rightarrow A\Psi^K_Q \qquad \text{with even } K, \tag{2.4}$$

$$\Psi^K_Q \rightarrow B\Psi^K_Q \qquad \text{with odd } K, \tag{2.5}$$

$$\Psi^{K,u}_Q \rightarrow B\Psi^{K,u}_Q, \tag{2.6}$$

$$\Psi^{K,g}_Q \rightarrow A\Psi^{K,g}_Q. \tag{2.7}$$

For reflections of the type $(0k0)$, the complex quantities $A$ and $B$ in these model structure factors are

$$\left.\begin{matrix} A \\ B \end{matrix}\right\} = p_1 \exp(\mathrm{i}\phi_1) \pm \{p_2 \exp(\mathrm{i}\phi_2) + p_3 \exp(\mathrm{i}\phi_3)\}, \tag{2.8}$$

where $\phi_j = 2\pi k y_j$ and $y_1 = 0.5827$, $y_2 = 0.7992$ and $y_3 = 0.3067$. Some values of $A$ and $B$ are listed on table 1.

Our model of gallium ferrate, which is defined in terms of (2.4)–(2.8), is fully compliant with elements of symmetry in the space group $Pc2_1n$ and, also, the established signatures of polar and magnetic order, although the model falls short of recognizing differences between cation environments in the three groups of cations. Of note is empirical evidence that Fe1 and Fe2 ions are located in distorted oxygen octahedra with different displacements from the centre of the octahedron along the $b$-axis estimated at +0.26 Å and −0.11 Å, respectively [5].

## 3. Bulk properties

Bulk properties of interest are related to structure factors in (2.4)–(2.7) evaluated with the Miller index $k = 0$, for which $A = 1.82$ and $B = -0.28$.

The bulk ferrimagnetic moment is proportional to (2.5) with $K = 1$ and it can be different from zero for $Q = 0$. The bulk magnetization in our model is therefore parallel to the axis of quantization, which coincides with the $c$-axis. Polar and anapole order parameters are proportional to (2.6) and (2.7) with $K = 1$, respectively. Both (2.6) and (2.7) with $K = 1$ vanish unless $Q = \pm 1$, and the electric polarization is parallel to the $b$-axis and the anapole moment is parallel to the $a$-axis.

Structure factors for bulk properties are also directly related to dichroic signals. We shall now switch attention to dichroism and discuss data gathered in the optical and x-ray regions with an alternating magnetic field applied along the $c$-axis and normal to the direction of the photon beam [6, 7].

## 4. Dichroic signals

For parity-even events E1–E1 and E2–E2, dichroic signals that couple to time-odd electron properties are allowed when helicity (Stokes parameter $P_2$) is present in the photon beam. In the measurements we aim to analyse [6, 7], only linear polarization is present, $P_2 = 0$, and subtraction of data collected in magnetic fields of opposite polarity singles out time-odd electron properties in the signals. Dichroic signals that are allowed under these experimental conditions include signals that are created in parity-odd events, with the electric dipole process (E1, parity-odd) in tandem with an electric quadrupole process (E2, parity-even) [9, 10, 14] or a magnetic dipole process (M1, parity-even) [9, 11, 13]. In both events, E1–M1 and E1–E2, time-odd electron properties manifest themselves in magnetoelectric multipoles, $\langle G^K_Q \rangle$, and their structure factors $\Psi^{K,g}_Q$ defined through (2.7) and (2.8).

Radial integrals are important factors in determining signal strengths. An E1 process contributes the integral $\{R\}_{\rm sp}$ and an E2 process contributes $\{R^2\}_{\rm sd}$, where the subscripts are appropriate in the context of the current application to s-, p- and d-type orbitals. We will measure these integrals in units of the Bohr radius, $a_0$. The M1 process between stationary states of an isolated ion is forbidden because the radial overlap of initial and final states in the process is zero, on account of their orthogonality. For an M1 process in a compound, the radial integral, denoted here by $\{1\}_{\gamma\gamma}$, is an overlap of two orbitals of the same angular momentum, $\gamma$, with components which may be centred on different ions. The magnitude of $\{1\}_{\gamma\gamma}$ is essentially a measure of configuration interactions and bonding, or covalency, of a cation and ligands. In order to express various contributions to a dichroic signal in the same unit, the classical radius of the electron $r_{\rm e} = \alpha^2 a_0$, we are obliged to introduce to E1–E2 and E2–E2 events a dimensionless factor $(m\Delta a_0^2/\hbar^2)$ where $\Delta$ is the energy of the photon event.

We use axes $(xyz)$ to describe the experimental apparatus. Let the direction of the photon beam, with a wavevector $\mathbf{q}$, define the $z$-axis and choose the $x$-axis parallel to linear polarization with Stokes parameter $P_3 = +1$, which is often called $\sigma$-polarization [14].

Field differences in dichroic signals are denoted by $\Delta Z$(E1–M1) and $\Delta Z$(E1–E2) and we choose to express them as

$$\Delta Z(\text{E1–M1}) = (q\{R\}_{\rm sp}\{1\}_{\gamma\gamma})\Delta F(\text{E1–M1})$$

and

$$\Delta Z(\text{E1–E2}) = (q\{R^2\}_{\rm sd}\{R\}_{\rm sp}/a_0^2)(m\Delta a_0^2/\hbar^2)\Delta F(\text{E1–E2}).$$

Following calculations reported in [13, 14], appropriate expressions for the key, dimensionless quantities $\Delta F(\text{E1–M1})$ and $\Delta F(\text{E1–E2})$ are

$$\Delta F(\text{E1–M1}) = -\hat{q}\left\{\sqrt{2}\Psi_0^{1,g} + \mathrm{i}P_3(\Psi_{+2}^{2,g} - \Psi_{-2}^{2,g})\right\} \tag{4.1}$$

and

$$\Delta F(\text{E1–E2}) = \hat{q}(\sqrt{3}/5)\left\{\Psi_0^{1,g} - \sqrt{(2/3)}\Psi_0^{3,g}\right\} + \hat{q}P_3(1/2)\left\{\mathrm{i}(\Psi_{-2}^{2,g} - \Psi_{+2}^{2,g}) + \sqrt{2}(\Psi_{-2}^{3,g} + \Psi_{+2}^{3,g})\right\}. \tag{4.2}$$

Contributions to (4.1) and (4.2) which are independent of linear polarization represent magnetochiral dichroism (M$\chi$D) and remaining contributions represent non-reciprocal linear dichroism (NRLD).

Rotation of the sample about the direction of the beam, **q**, does not change M$\chi$D. This follows because rotation of a spherical tensor by $\psi$ about the $z$-axis (which is the component 0 in the spherical basis) does nothing more than multiply the tensor by a phase factor $\exp(\mathrm{i}Q\psi)$ and for M$\chi$D one has $Q = 0$. NRLD has projections $Q = \pm 2$ and thus rotation of the sample by $\pi/2$, say, about **q** changes the sign of NRLD. Rotation of the sample by $\pi$ about either $x$- or $y$-axis changes the sign of $\Delta F(\text{E1–M1})$ and $\Delta F(\text{E1–E2})$. To see this first consider rotation by $\pi$ about the $x$-axis, and recall from section 2 that the operation $C_{2x}$ $(=C_{2a})$ applied to a spherical tensor results in a change in sign of its projection and a phase factor $(-1)^K$. When applied to (4.1) or (4.2), $C_{2x}$ does nothing more than produce an overall change of sign. The operation of $C_{2y}$ on a spherical tensor is the same as $C_{2x}$ apart from an additional phase factor $(-1)^Q = 1$ where the equality is correct for $Q = 0, \pm 2$.

Applied to $GaFeO_3$, we anticipate that expression (4.1) for the integrated E1–M1 dichroic signal represents observations of dichroism in the optical region [7], and that expression (4.2) for the integrated E1–E2 dichroic signal represents observations made in the vicinity of the Fe K edge [6]. Properties of magnetoelectric signals with respect to rotations of the sample, which are reviewed in the preceding paragraph, are certainly fully consistent with observations. In both experiments, a single crystal was mounted with its $a$-axis parallel to the beam and an alternating magnetic field parallel to the $c$-axis.

For this setting of the crystal and an E1–M1 event, M$\chi$D and NRLD, respectively, are proportional to $\Psi_0^{1,g} = 4A\langle G_a^1\rangle$ with $\langle G_a^1\rangle$ the component of the anapole moment parallel to the crystal $a$-axis, and $\mathrm{i}(\Psi_{+2}^{2,g} - \Psi_{-2}^{2,g}) = -8A\ \mathrm{Im}\langle G_{+1}^2\rangle_{abc}$ with the imaginary part of $\langle G_{+1}^2\rangle_{abc}$ the $zy$-component of the magnetoelectric quadrupole moment. In the optical region [7], the sign of the observed magnetoelectric multipoles was reversed by a rotation of the crystal by $\pi$ about the field direction normal to **q**. In addition, use of unpolarized light ($P_3 = 0$) isolated the M$\chi$D contribution. The two contributions to $\Delta F$ are separated by adding and subtracting spectra reported for orientations of the crystal that differ by a rotation of $\pi/2$ about the $a$-axis, since the rotation leaves M$\chi$D unchanged while the NRLD contribution changes sign. An E1–M1 event is held accountable for circular dichroism previously observed with molecules in random orientation [15]. In this case, the observed signal is created by parity-odd and time-even multipoles, $\langle U_Q^K\rangle$.

Should the cation site be a centre of inversion symmetry both M$\chi$D and NRLD are forbidden, whether one uses a crystal field or the molecular orbital method or some combination of the two. Even so there is merit, by way of an orientation, in considering symmetry properties of the electronic factor in the dichroic signals (4.1) and (4.2) when the six ligand ions form a regular octahedron and the symmetry is exactly cubic, with elements of symmetry in the full cubic group $O_\mathrm{h}$. In this hypothetical case, of full cubic symmetry, factors in M$\chi$D and NRLD attributed to the sample transform as the $\Gamma_{4-}$ and $\Gamma_{5+}$ representations, respectively [16]. $\Gamma_{4-}$ is spanned by $z$, etc and $\Gamma_{5+}$ is spanned by functions $xy$, etc. Behaviour of the signals with

respect to rotations of the sample relative to the apparatus, mentioned above, can be deduced from these functions. For the optical and x-ray regions, events of interest are allowed for augmented valence states formed by admixing p and d orbitals on the central atom with ligand orbitals. Admixtures permitted in full cubic symmetry have central atom 4p states admixed with ligand s and p orbitals ($\sigma$ are hybrid s–p ligand orbitals, and $\pi$ are p ligand orbitals) and central atom 3d states admixed with ligand p orbitals ($\pi$) and s and p orbitals ($\sigma$). If cation sites contain no centre of symmetry, which is the case for $GaFeO_3$, the crystal-field potential contains an odd part that mixes orbitals of opposite parity [17]. States in the pre-edge region of admixed s–p–d symmetry with increasing energy likely become pure s-like and, finally, pure p-like.

## 5. Resonant Bragg diffraction

In the diffraction experiment of interest [8], the primary $\sigma$-polarization is normal to the plane of scattering and parallel to the magnetic easy axis of the sample, $GaFeO_3$. No analysis was applied to states of polarization in the secondary beam and, thus, the detector recorded all possible states, $\sigma'$–$\sigma$ and $\pi'$–$\sigma$. An alternating field operates along the easy axis. The crystal was oriented for reflections $(0k0)$ where $k$ is an even integer, and the reflections are allowed by the space group.

The x-ray scattering length calculated to first order in the small quantity $E/mc^2$, where $E$ is the x-ray energy, is a sum of three amplitudes [18] with the leading part from Thomson scattering by electron charges. The Thomson amplitude is denoted by $F_c$ and it is different from zero in all observed reflections. A second amplitude depends on $E$ just through $E/mc^2$ and it is due entirely to the scattering of photons by electron spins. The third amplitude can enhance scattering when $E$ coincides with the energy of an atomic resonance. $F_c$ plus the resonant amplitude is identical to the Kramers–Heisenberg result, in the absence of electron spin, **s**. The spin does contribute in the resonant amplitude, where it appears in the current operator $= \{\mathbf{p} + \mathrm{i}\hbar\mathbf{s} \times \mathbf{q}\} \exp(\mathrm{i}\mathbf{q} \cdot \mathbf{R})$, with **p** the momentum conjugate to the position **R** of an electron.

The non-resonant spin amplitude is proportional to the vector product of primary and secondary polarization vectors projected on to the spin magnetization, here parallel to the primary polarization. The projection is identically zero, of course. The appropriate scattering length for the experiment is just the sum of $F_c$ and the resonant amplitude, which explicitly includes the spin magnetization. The orbital angular momentum of an electron, $\mathbf{R} \times \mathbf{p}$, appears in the resonant amplitude with the development in powers of **q** of the current operator, where it appears alongside the E2 process.

To make sense of their data, Arima *et al* [8] use a spin amplitude which is a sum of spin contributions to the current operator, extracted from the resonant amplitude by taking the limit $E \to \infty$ [19], and the non-resonant spin amplitude that is actually zero in their experiment. Di Matteo and Joly [20], in their analysis of the diffraction data, follow Arima *et al* [8] in using the same spin amplitude and fail to get agreement with data.

Arima *et al* [8] find resonance enhanced diffraction at the pre-edge to Fe K-shell absorption, and the enhancement is attributed to an E2 process. Using structure factors for our model, calculations outlined in appendix demonstrate that there is no contribution to diffraction from the parity-even event E2–E2 in the rotated channel of polarization, $\pi'$–$\sigma$, and the same, null result in the $\pi'$–$\sigma$ channel is obtained for all events under consideration. The E2–E2 event provides scattering in the unrotated channel of polarization, $\sigma'$–$\sigma$, with contributions from electron charge and magnetization. Also, the E1–E2 event provides scattering in this channel with contributions from polar and magnetoelectric multipoles. In the vicinity of the E2

resonance at an energy $\Delta_2$, the scattering length is of the form $F_c + d_2\{Z(\text{E2–E2}) + Z(\text{E1–E2})\}$ with $d_2 = \Delta_2/[E - \Delta_2 + \mathrm{i}\Gamma_2/2]$, plus a contribution from the E1 process at the higher energy $\Delta_1$. The non-resonant spin amplitude does not appear in our scattering length because it is identically zero when the spin magnetization is parallel to the primary polarization, as we mentioned before.

The E1–E1 event contributes charge scattering in the $\sigma'$–$\sigma$ channel but there is no magnetic (time-odd) scattering for primary $\sigma$-polarization. We find it is essential to a successful analysis to include the E1–M1 event with vital roles played by both contributions to the event, polar and magnetoelectric. The E1–M1 event can contribute in the $\sigma'$–$\sigma$ channel, and it is forbidden in the $\pi'$–$\sigma$ channel. In total, the contribution made by E1 processes to the $\sigma'$–$\sigma$ channel scattering length is $d_1\{Z(\text{E1–E1}) + Z(\text{E1–M1})\}$ where $d_1 = d_1' + \mathrm{i}d_1'' \approx d_1'$ with the approximation good for $\Delta_1 - \Delta_2 \gg \Gamma_1$.

Calculations with our model, which are reported in appendix, reveal that

$$Z(\text{E1–E1}) = Ah_c,$$
$$Z(\text{E1–M1}) = \mathrm{i}Bh_u + Ah_g,$$
$$Z(\text{E2–E2}) = Af_c + \mathrm{i}Bf_m$$

and

$$Z(\text{E1–E2}) = \mathrm{i}Bf_u + Af_g,$$

with the complex factors $A$ and $B$ defined in (2.8), and $f$s and $h$s purely real multipoles of the type indicated by subscripts. The calculations also provide the dependence of $h$s and $f$s on the Bragg angle, $\theta$. We find $h_u \propto \sin\theta$, $h_g \propto \cos\theta$, $f_c \propto \cos 2\theta$, $f_m \propto \sin 2\theta$, $f_u \propto \sin\theta$, $f_g \propto \cos\theta$, and $h_c$ is a constant independent of $\theta$. All the foregoing proportionalities are correct, apart from that for $f_c$ which depends on negligible angular anisotropy in the charge distribution of the S-state Fe ions.

Intensity of a resonance enhanced Bragg reflection found in the unrotated channel of polarization, $\sigma'$–$\sigma$, is

$$I = |F_c + d_2\{Z(\text{E2–E2}) + Z(\text{E1–E2})\} + d_1\{Z(\text{E1–E1}) + Z(\text{E1–M1})\}|^2. \tag{5.1}$$

In this expression, complex quantities are $A$, $B$, $d_2$ and $F_c$ and they are all expressed with the phase relation in $A = A' + \mathrm{i}A''$ with $A'$ and $A''$ purely real.

The quantity reported by Arima *et al* [8] is the difference in $I$ measured in applied fields of opposite polarity. This difference in intensities, $\Delta I$, contains many terms but the dependence of $\Delta I$ on x-ray energy is simplified by the mutual cancellation of all terms of the form $d_2'd_2''$. By construction, $\Delta I$ is proportional to time-odd multipoles whose sign is that of the applied field. Of these time-odd multipoles, we anticipate $f_m$ is very small, because for an event at the K edge $f_m$ is proportional to the orbital moment of the resonant 3d transition ion [21] which here is an S-state ion $Fe^{3+}$.

Taking $f_m = 0$ leaves $\Delta I$ proportional to sums of $f_g$ and $h_g$. As shown in appendix, these parity-odd multipoles, together with $f_u$ and $h_u$, undergo in $I$ a change of sign when the crystal is rotated by $\pi$ about the field direction, normal to the plane of scattering, and likewise our expression for $\Delta I$ succumbs to the change of sign. The specified rotation of the crystal takes the setting for the reflection $(0k0)$ to the setting for $(0\bar{k}0)$. The described behaviour of $\Delta I$ is in complete accord with observations. Data reported for the Bragg reflections (040) and $(0\bar{4}0)$ [8], and reproduced in figure 2, show that $\Delta I$ at the two reflections are essentially equal in magnitude and opposite in sign. In our calculation, magnitudes of $\Delta I$ at (040) and $(0\bar{4}0)$ are different because of expected differences in $F_c$ at the two reflections, which are illustrated in table 1.

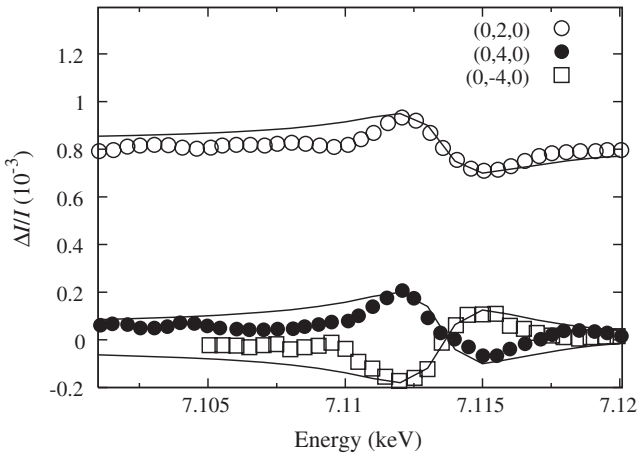


**Figure 2.** Experimental data for $\Delta I/I$ shown here for gallium ferrate are reported by Arima *et al* [8]. The sample temperature is 50 K, and intensities are for reflections $(0k0)$ with Miller indices $k = 2, 4$ and $-4$. Continuous curves are $\Delta I/2|F_c|^2$ with $\Delta I$ calculated from the expression (5.2). Quantities needed in $J$ are listed in table 1.

Our expression for $\Delta I$ with the simplifications $f_u = f_g = 0$, in keeping with $f_m = 0$, is in excellent agreement with experimental data. Figure 2 contains the function $\Delta I/2|F_c|^2$ evaluated for the reflections (020), (040) and $(0\bar{4}0)$ where

$$\Delta I = 4d_1' h_g \{J + f_c|A|^2 d_2'\} \tag{5.2}$$

and

$$J = A'F_c' + A''F_c'' + d_1'[h_u(-A'B'' + A''B') + h_c|A|^2].$$

The dependence of $\Delta I$ on $E$ is $d_2' = \Delta_2(E - \Delta_2)/[(E - \Delta_2)^2 + (\Gamma_2/2)^2]$ with $\Delta_2 = 7113.5$ and $\Gamma_2 = 3.0$ eV. Note that Arima *et al* [8] report difference data normalized by the measured total intensity, although from the text we understand the normalization is actually twice the total intensity. In our fit to data we normalize our calculated $\Delta I$ by $2|F_c|^2$.

A superior description of the energy dependence of $\Delta I$ is possible with $f_u \neq 0$, for then $\Delta I$ contains both $d_2'$ and $d_2''$ with $d_2'$ multiplied by $[f_u(-A'B'' + A''B') + f_c|A|^2]$. However, the very simple expression (5.2) with $f_u = 0$ is adequate for a first demonstration of the truth of our analysis, although the absence of $f_u$ somewhat distorts the proper physical significance of $f_c$.

Values for $A$ and $B$ for $(0k0)$ are obtained from (2.8) and table 1. At $(0\bar{k}0)$ the correct quantities are $A^*$ and $B^*$. Values of the Thomson structure factor were calculated with a routine that was checked against the Cambridge Crystallographic Subroutine Library, and input data was taken from Arima *et al* [5]. Our results for $F_c$ agree with those tabulated by Abrahams *et al* [22]. Values of $F_c'$ and $F_c''$ needed in the present calculations are listed in table 1.

Let us consider other quantities that appear in $\Delta I/2|F_c|^2$. A fit of this function to data, figure 2, was accomplished simply on the basis of the observed extrema in data at $E = 7112$ and 7115 eV. Data for a reflection $(0k0)$ provides one relation between $J$ and $f_c$, and one relation between $f_c$ and $d_1' h_g$, and only $d_1'$ is independent of the Miller index. In addition to six pieces of information from three reflections, we have calculated values for $A$, $B$ and $F_c$. The value extracted from the fit to data for the ratio $f_c(020)/f_c(040) = 1.26$ is in excellent agreement with the ratio of $\cos 2\theta$ at the two reflections, which is the functional dependence anticipated on the basis of our calculation ($\sin\theta = k\lambda/2b$ and $\lambda/2b = 0.093$). We also obtain the estimate

$f_c(020) \approx -0.014$, with the sign determined by the absolute sign of $\Delta I$ which is not known to us. Remaining multipoles in $\Delta I$ occur together with a factor $d_1' = -\Delta_1/(\Delta_1 - \Delta_2) \approx -300$. We find, $d_1' h_c \approx -0.30$, $d_1' h_u(020) \approx 67.0$, and $d_1' h_g(020) \approx 0.020$. The relatively large value of $h_u$ fits with the known large Fe displacement from the centre of the oxygen octahedron along the $b$-axis [5], and the magnetoelectric effect [3, 5].

As a guide to the values expected for $h_c$ and $f_c$ we calculate corresponding quantities for K-shell absorption by an *isolated* ion with the electron configuration $^6$S. In this extreme case, parity-even multipoles with $K > 0$ vanish, because the orbital angular momentum is exactly zero. The only multipole that contributes is

$$\langle T_0^0 \rangle = 1/\sqrt{(2l+1)}, \tag{5.3}$$

where $l$ is the angular momentum of the valence shell. We find

$$h_c = (4/3)(\{R\}_{\rm sp}/a_0)^2 (m\Delta a_0^2/\hbar^2), \tag{5.4}$$

and

$$f_c = (1/15)(q\{R^2\}_{\rm sd}/a_0)^2 (m\Delta a_0^2/\hbar^2) \cos 2\theta. \tag{5.5}$$

If the magnitude of $f_c$ in (5.5) is taken to be 0.014, implied by the foregoing analysis of data, one finds $\{R^2\}_{\rm sd}/a_0^2 \approx 0.015$ which is a factor 5.8 larger than an estimate of the radial integral made with hydrogen wavefunctions and a charge $= 26$, and 16.0 larger than the estimate obtained from an atomic code [23]. The atomic code estimates $\{R\}_{\rm sp}/a_0 = 0.0035$ and with this value (5.4) yields $d_1' \approx -68$. These findings reinforce the notable successes of (5.2), with its excellent description of experimental data together with transparency as to its physical content.

To round off this section on resonant Bragg diffraction we discuss differences between our analysis and the one offered by Arima *et al* [8]. These authors aim to make sense of two principal features in their data, reproduced in figure 2: (i) a magnetic background that depends weakly on the x-ray energy, and (ii) similar peak-to-peak values of normalized resonant intensities at (020) and (040). Arima *et al* [8] appeal to the purely (spin) magnetic, high-energy limit of the scattering length to estimate feature (i), and then turn to a parity-odd and time-odd contribution to resonant scattering from the E1–E2 event (a contribution here denoted by $f_g$) to estimate feature (ii). Of course, all features in the data, including (i) and (ii), must derive from a single unique scattering length, to be found in cited references [18]. An achievement of our work is a unified, rather than piecemeal, analysis of the data. It immediately reveals important interference contributions to scattering. We also nicely describe the energy dependence which Arima *et al* [8] do not mention in their analysis.

In our analysis, interference between Thomson scattering and the low-energy tail of the E1–M1 resonant event, proportional to $h_g$, accounts for feature (i). Among values for the multipoles inferred from data $h_g$ is by far the smallest multipole, a finding which fits with what is anticipated from a magnetic event that involves M1. Interference is also responsible for feature (ii). Referring to (5.2), the peak-to-peak value at resonance is determined by interference of charge scattering in E2–E2, $f_c A(0k0)$, and magnetoelectric scattering in E1–M1, $h_g A(0k0)$. The ratio of $h_g f_c |A(0k0)|^2 \propto \cos(\theta)\cos(2\theta)|A(0k0)|^2$ between (020) and (040) is 0.09, that together with normalization $|F_c(040)|^2/|F_c(020)|^2 = 8.9$ gives a ratio 0.83 between the normalized peak-to-peak resonant intensities at the two reflections, in complete accord with data. Note that this good result depends simply on the derived Bragg-angle dependence of the charge and magnetoelectric multipole contributions to scattering, not on the inferred magnitude of multipoles, which builds confidence in the truth of our analysis.

## 6. Conclusions

We have constructed an atomic model of Fe ions in gallium ferrate ($GaFeO_3$) and used it to analyse observations made on the exemplar multiferroic compound with optical and x-ray techniques. While held at a low temperature, $GaFeO_3$ hosts spontaneous polar and magnetic order [1], and the magnetoelectric effect [3, 5]. A pyroelectric effect in $GaFeO_3$ which is allowed by the polar crystal class, $C_{2v}$, has not been observed, to the best of our knowledge.

Use in recent experiments [6–8] of a single crystal of gallium ferrate experiencing an applied magnetic field permits an unambiguous isolation of electron properties that are changed on reversal of the direction of time. In our analysis, electron properties with this time signature are expressed in terms of magnetic multipoles, and magnetoelectric multipoles that do not exist in a compound with a centrosymmetric structure. Dichroism observed in the energy interval 1.0–2.5 eV [7] and near the Fe K edge [6] is here attributed entirely to parity-odd, time-odd magnetoelectric multipoles. In fact, observed signals are the sum of two non-reciprocal dichroic signals often called magnetochiral and non-reciprocal linear dichroic signals.

Bragg diffraction enhanced by a resonance near the Fe K edge [8], according to our analysis, includes interference between Thomson scattering and E1, M1 and E2 absorption processes, which has not hitherto been observed. The E1–M1 event is important in practice for events forbidden by the selection rules for pure electric processes, which indeed is the case. By successfully comparing our calculated intensity with experimental data we demonstrate in diffraction the pivotal role played by polar and magnetoelectric contributions from the E1–M1 event, both of which only exist because $GaFeO_3$ possesses a non-centrosymmetric structure. The polar contribution is found to be relatively large, which fits nicely with a measured large magnetoelectric effect [3, 5] and measured large displacements of Fe ions from centres in iron–oxygen octahedral units [5].

### Acknowledgments

We are grateful to Professor Gerrit van der Laan who provided us with radial integrals, and Dr T Arima for permission to reproduce diffraction data in [8]. Dr Javier Fernández Rodríguez prepared figure 2.

### Appendix. Unit cell structure factors

We describe calculations of unit cell structure factors, $F$, using previous analytic results for the scattering length, which is expressed in units of $r_e$ [13, 14]. The structure factors provide the functions that appear in (5.1), namely,

$$Z(\text{E1–E1}) = (\{R\}_{\text{sp}}/a_0)^2(m\Delta a_0^2/\hbar^2)F(\text{E1–E1}) = Ah_c,$$
$$Z(\text{E1–M1}) = (q\{R\}_{\text{sp}}\{1\}_{\gamma\gamma})F(\text{E1–M1}) = \text{i}Bh_u + Ah_g,$$
$$Z(\text{E2–E2}) = (q\{R^2\}_{\text{sd}}/a_0)^2(m\Delta a_0^2/\hbar^2)F(\text{E2–E2}) = Af_c + \text{i}Bf_m$$

and

$$Z(\text{E1–E2}) = (q\{R^2\}_{\text{sd}}\{R\}_{\text{sp}}/a_0^2)(m\Delta a_0^2/\hbar^2)F(\text{E1–E2}) = \text{i}Bf_u + Af_g,$$

with $a_0$ the Bohr radius. All scattering occurs in the unrotated channel of polarization, as we shall see.

The generic form of a parity-even unit cell structure factors is

$$F = \sum_K \mathbf{X}^K \cdot \mathbf{D}^K \cdot \mathbf{\Psi}^K. \tag{A.1}$$

The three spherical tensors of rank $K$ in (A.1) are as follows: $\mathbf{X}^K$ describes properties of the x-ray beam, $\mathbf{D}^K$ is a rotation that establishes the setting of the crystal with respect to axes that define the plane of scattering and states of polarization, and $\mathbf{\Psi}^K$ is a structure factor from section 2. Values of $\mathbf{X}^K$ that are appropriate for E1–E1 and E2–E2 events are listed in [14]. Following the convention in [14], we define axes $(xyz)$ for the experiment such that, the plane of scattering is spanned by $x$–$y$, with the Bragg wavevector $(hkl)$ in the opposite direction to the $x$-axis, and $\sigma$-polarization parallel to the $z$-axis. In the experiment of interest, the $c$-axis is parallel to the $z$-axis so $\mathbf{D}^K$ makes $(0k0)$ parallel to $-x$ with a rotation by $\pi/2$ about the $c$-axis and it amounts to a simple multiplicative phase factor $\exp(\mathrm{i}Q\pi/2)$.

Taking $X^K_Q$ from [14] a simple calculation leads to,

$$\begin{aligned} F_{\sigma'\sigma}(\text{E1–E1}) &= \sum_{KQ}(-1)^Q X^K_{-Q}\mathrm{e}^{\mathrm{i}Q\pi/2}\Psi^K_Q \\ &= \left\{X^0_0\Psi^0_0 + X^2_0\Psi^2_0\right\}, \end{aligned} \tag{A.2}$$

which is independent of the Bragg angle, $\theta$. From (2.1) and (2.4),

$$\Psi^K_0 = 2[1+(-1)^k]A\langle T^K_0\rangle, \tag{A.3}$$

and contributions to scattering occur for even $k$. $F_{\pi'\sigma}(\text{E1–E1})$, and $F_{\pi'\sigma}(\text{E2–E2})$, contain $\Psi^K_Q$ with odd $Q$ and it vanishes for even $k$. In the unrotated channel the unit cell structure factor for an E2–E2 event is

$$\begin{aligned} F_{\sigma'\sigma}(\text{E2–E2}) = \frac{1}{2\sqrt{5}}\cos(2\theta)\left[\Psi^0_0 - \sqrt{\frac{5}{14}}\Psi^2_0 - 2\left(\frac{2}{7}\right)^{1/2}\Psi^4_0\right] \\ - \frac{1}{2}\left(\frac{3}{7}\right)^{1/2}\Psi^2_{+2} + \frac{1}{\sqrt{7}}\Psi^4_{+2} + \frac{\mathrm{i}}{2\sqrt{10}}\sin(2\theta)\left[-\Psi^1_0 + 2\Psi^3_0\right]. \end{aligned} \tag{A.4}$$

The results (A.2) and (A.4) establish properties of $Z(\text{E1–E1})$ and $Z(\text{E2–E2})$ that are used in section 5. As one example, we give the explicit expression for $f_m$ obtained from (A.4),

$$Bf_m = (q\{R^2\}_{\mathrm{sd}}/a_0)^2(m\Delta a_0^2/\hbar^2)\frac{1}{2\sqrt{10}}\sin(2\theta)\left[-\Psi^1_0 + 2\Psi^3_0\right], \tag{A.5}$$

where $\Psi^K_0$ with odd $K$ is taken from (2.1) and (2.5). For absorption at the K edge, $\langle T^1_0\rangle$ is proportional to the orbital angular momentum in the 3d shell, and $\langle T^3_0\rangle$ is proportional to the orbital octupole in the 3d shell [14, 21].

We have observed that parity-even contributions to $\pi'\sigma$ diffraction are forbidden because the x-ray factor in (A.1) is different from zero for odd $Q$ while $\Psi^K_Q$ given in (2.1) is identically zero for odd $k+Q$. A similar selection rule forbids parity-odd contributions to $\pi'\sigma$ diffraction. For E1–E2 and E1–M1 events the $\pi'\sigma$ x-ray factors are different from zero for even $Q$ while $\Psi^{K,u}_Q$ and $\Psi^{K,g}_Q$ given in (2.2) and (2.3), respectively, vanish for even $k+Q$. The absence of $\pi'\sigma$ diffraction is a consequence of the particular setting of the crystal and for Bragg reflections other than $(0k0)$ it can be different from zero.

The parity-odd unit cell structure factor $F_{\sigma'\sigma}(\text{E1–E2})$ is a linear combination of $\Psi^{K,g}_Q$ and $\Psi^{K,u}_Q$ with $K = 1, 2$ and 3 and $Q = \pm 1$. Using results in [14] we find,

$$\begin{aligned} F_{\sigma'\sigma}(\text{E1–E2}) = \tfrac{1}{5}\sqrt{6}\{\cos\theta\Psi^{1,g}_{+1} + \sin\theta\Psi^{1,u}_{+1}\} + \tfrac{4}{5}\left(\tfrac{2}{3}\right)^{1/2}\{\cos\theta\Psi^{3,g}_{+1} + \sin\theta\Psi^{3,u}_{+1}\} \\ + \mathrm{i}\left(\tfrac{2}{15}\right)^{1/2}\{\cos\theta\Psi^{2,g}_{+1} + \sin\theta\Psi^{2,u}_{+1}\} \end{aligned} \tag{A.6}$$

Contributions to $F_{\sigma'\sigma}(\text{E1–E2})$ by polar (magnetoelectric) multipoles have $\sin\theta$ ($\cos\theta$) as a common factor and they form $\mathrm{i}Bf_u$ ($Af_g$), where $f_u$ and $f_g$ are sums of purely real multipoles.

Multipoles in the E1–M1 event have rank $K = 0, 1$ and 2. However, $K = 0$ does not contribute in $F_{\sigma'\sigma}$(E1–M1) because $Q = \pm 1$. From results in [13] we are able to show that

$$F_{\sigma'\sigma}(\text{E1–M1}) = -2\{\cos\theta\,\Psi^{1,g}_{+1} + \sin\theta\,\Psi^{1,u}_{+1} - \mathrm{i}(\cos\theta\,\Psi^{2,g}_{+1} + \sin\theta\,\Psi^{2,u}_{+1})\}. \tag{A.7}$$

In common with (A.6), this expression is of the form $(\mathrm{i}Bh_u + Ah_g)$ in which $h_u$ and $h_g$ are purely real multipoles.

The setting of the crystal used to measure a reflection $(0 - k0)$ differs by a rotation of $\pi$ about the $z$-axis from the setting used above for the reflection $(0k0)$. Such a rotation makes two changes to structure factors (A.2), (A.4), (A.6) and (A.7). First $A \to A^*$ and $B \to B^*$ because the direction of the crystal $b$-axis is reversed by the rotation and $\phi \to -\phi$ in (2.8). Secondly, parity-odd unit cell structure factors change sign because the rotation about the $z$-axis introduces a phase factor $(-1)^Q$ and $Q = \pm 1$ in (A.6) and (A.7). Parity-even structure factors involve only even $Q$ and remain unchanged on rotation of the crystal.

## References


[1] Remeika J P 1960 *J. Appl. Phys.* **31** (Suppl) 263S
[2] Frankel R B *et al* 1965 *Phys. Rev. Lett.* **15** 958
[3] Rado G T 1964 *Phys. Rev. Lett.* **13** 335
[4] Wood E A 1960 *Acta Crystallogr.* **13** 682
[5] Arima T *et al* 2004 *Phys. Rev.* B **70** 064426
[6] Kubota M *et al* 2004 *Phys. Rev. Lett.* **92** 137401
[7] Jung J H *et al* 2004 *Phys. Rev. Lett.* **93** 037403
[8] Arima T *et al* 2005 *J. Phys. Soc. Japan* **74** 1419
[9] Carra P and Benoist R 2000 *Phys. Rev.* B **62** R7703
[10] Carra P *et al* 2003 *Phys. Rev.* B **67** 045111
[11] Marri I *et al* 2006 *J. Phys. A: Math. Gen.* **39** 1969
[12] Barron L D 2004 *Molecular Light Scattering and Optical Activity* (Cambridge: CUP)
[13] Collins S P *et al* 2007 *J. Phys.: Condens. Matter* **19** 213201
[14] Lovesey S W *et al* 2005 *Phys. Rep.* **411** 233
[15] Turchini S *et al* 2004 *J. Am. Chem. Soc.* **126** 4532
[16] Abragam A and Bleaney B 1970 *Electron Paramagnetic Resonance of Transition Ions* (Oxford: Clarendon)
Weissbluth M 1978 *Atoms and Molecules* (New York: Academic)
[17] Görller-Walrand C and Binnemans K 1996 *Handbook on the Physics and Chemistry of Rare Earths* vol 23 (Amsterdam: Elsevier Science)
Staub U and Soderholm L 2000 *Handbook on the Physics and Chemistry of Rare Earths* vol 30 (Amsterdam: Elsevier Science)
[18] Grotch H *et al* 1983 *Phys. Rev.* A **27** 243
Lovesey S W and Collins S P 1996 *X-ray Scattering and Absorption by Magnetic Materials* (Oxford: Clarendon) section 8.2
[19] de Bergevin F and Brunel M 1981 *Acta Crystallogr.* A **37** 314
[20] Di Matteo S and Joly Y 2006 *Phys. Rev.* B **74** 014403
[21] Lovesey S W 1998 *J. Phys.: Condens. Matter* **10** 2505
[22] Abrahams S C *et al* 1965 *J. Chem. Phys.* **42** 3957
[23] van der Laan G 2007 private communication